

# Liquid-Liquid Phase Transition in Simulated Supercooled Water Nanodroplets

Shahrazad M. A. Malek<sup>1</sup>,,<sup>1</sup> Francesco Sciortino<sup>2</sup>,,<sup>2</sup> Peter H. Poole<sup>3</sup>,,<sup>3</sup> and Ivan Saika-Voivod<sup>4</sup>

<sup>1</sup>Department of Physics, *University of the Fraser Valley*, Abbotsford, British Columbia V2S 7M7, Canada

<sup>2</sup>Dipartimento di Fisica, *Sapienza University of Rome*, 00185 Rome, Italy

<sup>3</sup>Department of Physics, *St. Francis Xavier University*, Antigonish, Nova Scotia B2G 2W5, Canada

<sup>4</sup>Department of Physics and Physical Oceanography, *Memorial University of Newfoundland*, St. John's, Newfoundland and Labrador A1B 3X7, Canada



(Received 19 September 2024; accepted 4 March 2025; published 31 March 2025)

Using simulations, we demonstrate how a liquid-liquid phase transition (LLPT) manifests in supercooled water nanodroplets. Selecting an interaction potential for which a LLPT occurs in the bulk liquid, we conduct simulations of supercooled water nanodroplets having between 1000 and 80000 molecules. We show that as the droplet size decreases, the Laplace pressure grows large enough to drive the droplets through the transition from the low-density to the high-density liquid phase, and that all droplets in this size range are large enough to have cores exhibiting the structure and properties of bulk water. To guide experiments, we estimate the range of values for the critical pressure of the LLPT in real water that can be observed using nanodroplets, and propose structural and dynamical measures by which the LLPT in nanodroplets can be detected.

DOI: [10.1103/PhysRevLett.134.138001](https://doi.org/10.1103/PhysRevLett.134.138001)

Despite more than 30 years of effort, experiments to confirm and locate the proposed liquid-liquid phase transition (LLPT) in supercooled water, which separates low-density liquid (LDL) and high-density liquid (HDL) phases, remain challenging [1–7]. This is due primarily to the regime of low temperature  $T < 220$  K predicted for the LLPT. At such extreme supercooling, the lifetime of the metastable liquid state prior to the onset of ice formation is on the order of 10  $\mu$ s in bulk water [6]. An additional complication is that estimates for both the temperature  $T_c$  and pressure  $P_c$  of the critical point that terminates the LDL-HDL coexistence line depend on the simulation model studied or on the method used to extrapolate experimental data below the homogeneous nucleation temperature [1,2,8–11].  $P_c$  values ranging from 10 to 200 MPa have been proposed, with recent predictions clustered around 100 MPa [12–15].

Recent experiments focus on approaches to address these challenges. For example, Nilsson and coworkers have exploited ultrafast laser pulses to simultaneously heat and pressurize bulk amorphous ice samples to the conditions of the LLPT, which are then probed by femtosecond x-ray laser pulses to capture evidence of the LLPT in the brief time window before the appearance of ice [6,7].

Such experimental results, while significant, are complex to interpret and do not yet provide a complete characterization of the LLPT, including precise estimates for  $T_c$  and  $P_c$ . Complementary approaches to test for the LLPT are therefore required.

One such approach, which exploits the properties of liquid water nanodroplets, was proposed in Ref. [16]. The strength of this proposal is that it exploits the characteristics of nanodroplets to avoid the challenges faced in studies of bulk water. The crystal nucleation rate for a sample of supercooled liquid is proportional to the sample volume. As a result, ice nucleation is significantly suppressed in nanodroplets compared to a bulk system at the same degree of supercooling. In addition, the Laplace pressure inside a liquid droplet varies as the inverse of the droplet radius. For nanoscale droplets, the Laplace pressure can be significant, creating the possibility to study the liquid under pressure without the need to impose pressure via external means.

Reference [16] used simulations of the TIP4P/2005 water model [17] to show that the density maximum, a well known anomaly of bulk water, is also observed in nanodroplets as small as a few hundred molecules. Reference [16] also showed that the Laplace pressure inside water nanodroplets can reach 200 MPa, and that indications of the LLPT, previously established to occur in bulk TIP4P/2005 water, are observed in the thermodynamic properties of nanodroplets. For TIP4P/2005, the estimate for  $P_c$  is 186 MPa [11]. In Ref. [16], attaining a Laplace pressure of 186 MPa required droplets having a number of molecules  $N$  on the order of 100. At such small sizes, surface effects dominate the properties of

Published by the American Physical Society under the terms of the [Creative Commons Attribution 4.0 International](https://creativecommons.org/licenses/by/4.0/) license. Further distribution of this work must maintain attribution to the author(s) and the published article's title, journal citation, and DOI.

nanodroplets, inducing significant deviations from bulk behavior. As a result, a sharp LLPT does not occur in TIP4P/2005 nanodroplets, but rather takes the form of a significantly rounded, continuous crossover in thermodynamic properties. Hence, if real water behaved in the same way as TIP4P/2005, nanodroplets could not be used to demonstrate the existence of the LLPT in bulk water.

However, recent studies suggest that  $P_c$  for real water may be significantly lower than in TIP4P/2005 [12–14]. If so, it then becomes important to explore the case in which  $P_c$  can be reached in nanodroplets having a bulklike interior. To do so, we choose the WAIL model of water, in which the LLPT has been observed at  $P_c = 37$  MPa and  $T_c = 210$  K [18,19]. Based on the results of Ref. [16], a Laplace pressure of 37 MPa will occur inside water nanodroplets containing on the order of  $N = 10^4$  molecules, a droplet size that provides a better promise of observing bulklike behavior, including a sharp LLPT. In the present work, we reveal the physics of a fully developed LLPT occurring in water nanodroplets.

The model we study, the WAIL potential, is a flexible and polarizable water model that uses parameters based on *ab initio* calculations [20]. We carry out molecular dynamics simulations using Gromacs v5.1.2 and v5.1.4 [21–26]. We model each molecule as  $D_2O$  to allow us to use a longer time step of 1 fs, instead of 0.5 fs, as used in Ref. [20]. In order to facilitate comparison with previous work, here we convert all density values to correspond to the molecular weight of  $H_2O$ . All our simulations use periodic boundary conditions and are conducted in the constant- $(N, V, T)$  ensemble, where  $V$  is the system volume, and where  $T$  is constrained using the Nosé-Hoover thermostat [27,28]. Long-range electrostatic contributions are evaluated using the Particle-Mesh Ewald method [29]. Further details on our methods are given in Supplemental Material (SM) [30].

Our runs simulate droplets of  $N$  molecules in a cubic simulation box with edge length  $L$  that is much larger than the expected droplet diameter. We are primarily interested in testing for bulklike properties occurring in the core of water droplets. To quantify the density of the liquid in the droplet core, we define  $\rho_{\text{core}} = mN_c/V_c$ , where  $N_c$  is the number of O atoms within  $r_c$  of the droplet center,  $m$  is the mass of a water molecule, and  $V_c = (4/3)\pi r_c^3$ . The value of  $r_c$  is chosen to be approximately one-half the droplet radius and is tabulated in Table S1.

Our simulations start from configurations created in three different ways. We use *de novo* (DN) configurations generated from random arrangements of molecules. We also create initial configurations at two different densities by carving out smaller droplets from the interior of our largest ( $N = 80000$ ) droplet during simulations at two temperatures, 210 and 230 K. “Initially low density” (ILD) droplet configurations with  $\rho_{\text{core}} = 0.926$  g/cm<sup>3</sup> are obtained from the 210 K run; “initially high density” (IHD) configurations with  $\rho_{\text{core}} = 1.025$  g/cm<sup>3</sup> are obtained from

the 230 K run. All results presented here are from runs conducted at 210 K (the estimated value of  $T_c$  for the WAIL model) initiated from one of these three types of configurations. Details for each run are provided in Table S1.

We monitor equilibration of our droplets from the time dependence of  $\rho_{\text{core}}$ , shown for each run in Fig. S1. We also evaluate a neighbor correlation function  $f(t)$  defined as the fraction of nearest neighbors that remain so over a time  $t$  [16]; see SM [30] for details. We fit a stretched exponential function to the decay of  $f(t)$  to obtain a relaxation time  $\tau$  for successive time windows. As shown in Fig. S2, all our runs are much longer than the largest  $\tau$  observed during the run. Despite this, the variation of  $\rho_{\text{core}}$  and  $\tau$  with time shows that several of our runs, particularly for the largest droplets, do not attain a stationary state on the time scale of our simulations. Assuming a monotonic decay to equilibrium, we use these runs to place a bound on the equilibrium value of  $\rho_{\text{core}}$  and  $\tau$ .

We define the droplet density profile  $\rho(r)$  as the density of molecules that have O atoms in a shell of radius  $r$ , as measured from the droplet center of mass evaluated using O atoms only. Density profiles at 210 K for droplets of three sizes are shown in Fig. 1(a). As noted in previous work on cold and supercooled water nanodroplets, we observe that the density near the droplet surface is higher than in the interior [16]. This effect is more pronounced for larger droplets at lower  $T$  for the following reasons. The core of a sufficiently large droplet will have bulklike properties, from which deviations are expected approaching the droplet surface. As  $T$  decreases below the density maximum of water, the density of the bulklike core will decrease. However, the formation of an open hydrogen bond network is always disrupted near the droplet surface. Therefore, cooling is less effective in lowering the density at the surface compared to the interior, creating a droplet with a denser outer shell surrounding a less dense core.

Figure 2(a) shows our equilibrium estimates for, or bounds on,  $\rho_{\text{core}}$  as  $N$  varies from 1000 to 80000. For our largest droplets, regardless of how they are initiated,  $\rho_{\text{core}}$  trends toward the predicted value of the bulk density 0.90 g/cm<sup>3</sup> for WAIL water at  $T = 210$  K at ambient pressure [19]. As  $N$  decreases, a rapid increase in  $\rho_{\text{core}}$  occurs in a narrow range near a critical value of  $N_c \simeq 15000$ . For droplets with  $N < N_c$ , and regardless of how they are initiated,  $\rho_{\text{core}}$  relaxes at long times to values in the range 1.0 to 1.1 g/cm<sup>3</sup>, much higher than the density of the bulk liquid at ambient pressure. This behavior is consistent with a LLPT from LDL to HDL occurring in the droplet core due to the increase in Laplace pressure as droplet size decreases. Significantly, for two runs initiated with ILD configurations,  $N = 8963$  and 13697, the behavior of  $\rho_{\text{core}}$  with time [Fig. S1(b), right panel] suggests that these droplets initially establish a metastable LDL core that subsequently undergoes a phase

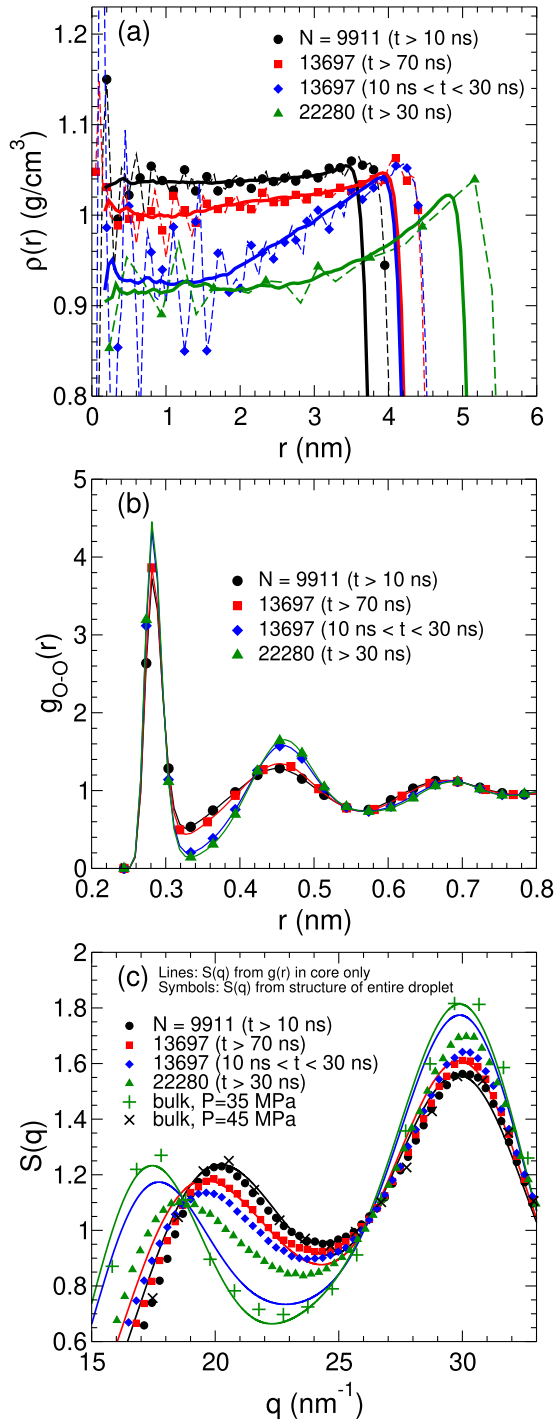


FIG. 1. (a) Density profiles  $\rho(r)$  (dashed lines with symbols) for several droplet sizes straddling the LLPT. In each case, the time window for averaging configurations is given. Thin lines show the density profiles evaluated using the Voronoi volumes around each molecule, as described in SM [30]. (b) Radial distribution function  $g(r)$  for O atoms in the droplet core. (c) Structure factor  $S(q)$  for O atoms. Small symbols show  $S(q)$  calculated directly from the positions of all atoms in the droplet. Lines show  $S(q)$  evaluated from the  $g(r)$  for core O atoms, as described in SM [30]. Large symbols show  $S(q)$  from bulk WAIL simulations reported in Ref. [18].

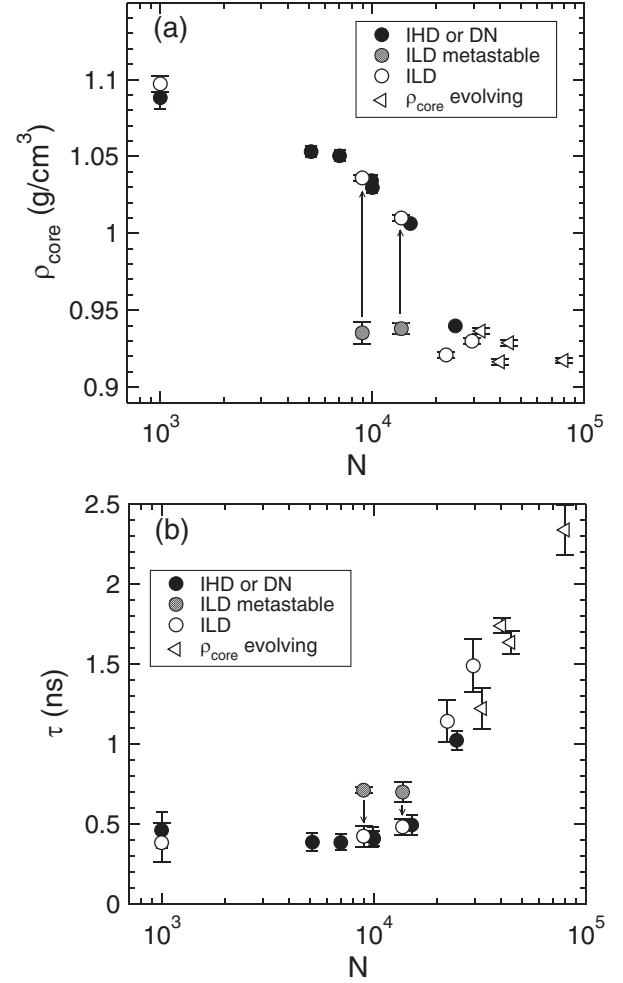


FIG. 2. (a)  $\rho_{\text{core}}$  and (b)  $\tau$  versus  $N$  at  $T = 210$  K. In both panels, circular symbols denote runs in which  $\rho_{\text{core}}$  is approximately stationary. The time windows for averaging each point are given in Table S1. As described in SM [30], three types of initial configurations are used in these runs: IHD and DN configurations (filled circles) and ILD configurations (open circles). Shaded circles indicate the early time properties of ILD-initiated runs that show evidence of metastability in the form of a low-density state at short time that transforms (see arrows) to a high density state at later time. Triangles locate an upper (lower) bound on  $\rho_{\text{core}}$  ( $\tau$ ) values for runs that have not reached equilibrium. Error bars are evaluated as described in SM [30].

change to HDL. Such metastability is a hallmark of a first-order phase transition.

Dynamical evidence for the LLPT is shown in Fig. 2(b). As  $N$  decreases, the neighbor relaxation time  $\tau$  decreases and drops sharply in the vicinity of  $N_c$ . This behavior is consistent with a phase transition from LDL to HDL as  $N$  decreases because bulk LDL is expected to have a significantly larger structural relaxation time than HDL [31]. We again find that the ILD-initiated  $N = 8963$  and  $13697$  runs show evidence of metastability, starting out with a larger  $\tau$  at early time, corresponding to the LDL

phase, and switching to smaller  $\tau$  at longer time, when HDL forms.

We next evaluate the pressure inside our droplets to quantify the magnitude of the Laplace pressure corresponding to the density change observed in Fig. 2(a). We define the pressure profile  $P(r)$  inside a droplet using the method described in Sec. 3.3 of Ref. [32]; see SM [30] for details.  $P(r)$  for a droplet with  $N = 1000$  is shown in Fig. S5. As found previously,  $P(r)$  is approximately constant in the droplet interior, becomes negative on approach to the surface and then decays to the ambient pressure of the vapor. We define  $P_{\text{core}}$ , the pressure in the droplet core, by averaging  $P(r)$  out to a radius  $r_{cp}$  within which we observe  $P(r)$  to remain approximately constant. The value of  $r_{cp}$  used for each droplet size is recorded in Table S1. Figure 3 plots the values of  $P_{\text{core}}$  versus  $\rho_{\text{core}}$  for each of our droplets, compared with the bulk behavior of  $P$  versus  $\rho$  reported in Ref. [18]. Within the error of our measurements, we find a good correspondence between the droplet and bulk behavior, confirming that the cores of all our droplets are large enough to express bulklike behavior. The value of  $P_{\text{core}} \simeq 40$  MPa at which the transition from LDL to HDL occurs in the cores of our droplets is consistent with  $P_c = 37$  MPa for the LLPT in bulk WAIL simulations. Note that the data in Fig. 3 show a clear inflection, consistent with the presence of a compressibility maximum as a function of the pressure (at constant  $T$ ).

The molecular structure in our droplet cores is also consistent with a LDL to HDL transition as  $N$  decreases. Figure 1(b) shows the radial distribution function  $g(r)$  for O-O pairs where at least one O atom is in the core. We show  $g(r)$  for several droplets straddling the phase change,

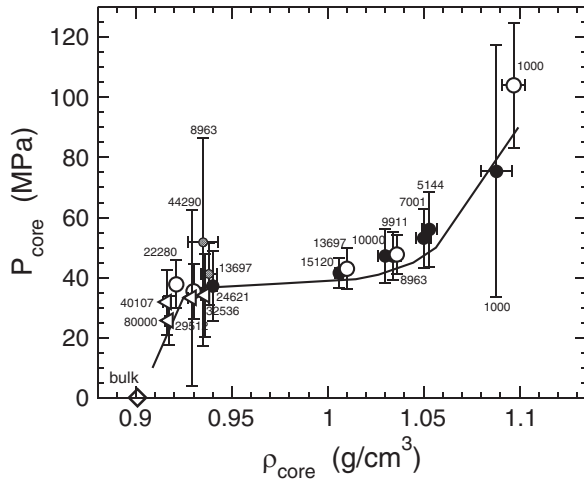


FIG. 3.  $P_{\text{core}}$  versus  $\rho_{\text{core}}$  at  $T = 210$  K. Nanodroplet size  $N$  is indicated for each data point. Symbols have the same meaning as in Fig. 2. The solid curve is the bulk equation of state estimated in Ref. [18]. The diamond indicates the density of the bulk liquid at ambient  $P$  evaluated in Ref. [19]. Error bars are  $\pm 2$  times the standard error, calculated as described in SM [30].

including our  $N = 13697$  run which starts in the LDL phase but then switches to the HDL phase. Droplets in the LDL phase show characteristically sharper first and second peaks in  $g(r)$  with a deep minimum in between; in the HDL droplets, these features are suppressed. Similarly, Fig. 1(c) shows that the structure factor  $S(q)$  for O atoms in our droplet cores compares well with  $S(q)$  of the bulk WAIL liquid, both in the LDL and HDL phases [18].

In summary, our simulations predict that when  $P_c = 37$  MPa, the LLPT will occur due to Laplace pressure in nanodroplets at a critical droplet size of  $N_c \simeq 15000$ . Our results also establish that bulklike behavior occurs in the cores of deeply supercooled water nanodroplets of size  $N \gtrsim 1000$ . We also find that the Laplace pressure in such droplets reaches as high as 100 MPa. Therefore, if  $P_c \lesssim 100$  MPa for the LLPT in real water, then experiments on water nanodroplets in vacuum have the potential to detect the LLPT.

By using the WAIL model, with its low value of  $P_c$ , we have shown that a fully developed LLPT can occur in a water nanodroplet. Nonetheless,  $P_c$  may be higher than in the WAIL model. For example,  $P_c = 90$  MPa for the updated rWAIL model [33] and  $P_c = 105$  MPa for the neural network version of the MB-pol model [12]. Using Laplace pressure alone to reach this range of  $P_c$  will require the study of small droplets of size  $N \sim 1000$ , which presents experimental challenges. To address this, we note that the Laplace pressure adds to the pressure of the medium, which in the present work is effectively a vacuum. Investigating nanodroplets surrounded by a pressurizable inert medium may provide a method to tune the pressure in the droplet core to arbitrary values. In this way, much larger droplets, which are easier to produce and more assuredly bulk-like, could be used to test for the LLPT even if  $P_c > 100$  MPa.

A range of other experimental approaches could be used to detect the LLPT using nanodroplets. For example: (i) Hyperquenched nanodroplets deposited on a cold surface should produce a low-density aggregate when  $N > N_c$ , and a high-density aggregate when  $N < N_c$ . (ii) Experiments that probe the structure of individual droplets, such as those described in Ref. [5], will have to account for the influence of the surface layer of the droplets, which, as we have seen, is not necessarily bulk-like. In Fig. 1(c), we compare the  $S(q)$  calculated when only core molecules are considered, and when all the molecules in the droplet are used. When all molecules are used, the characteristic increase in the  $q$  value of the first sharp diffraction peak as the system changes from LDL to HDL is still present, but is decreased in magnitude, compared to the  $S(q)$  behavior when only core molecules are used. Whether this less dramatic shift can be detected in scattering experiments on nanodroplets will depend on the sensitivity of the measurements. (iii) Estimation of the droplet density, and its variation with  $N$ , using the predicted



shape of  $S(q)$  at small  $q$  for droplets may also be feasible in experiments [34–36]. (iv) The abrupt decrease in the relaxation time of nanodroplets as  $N$  decreases can also be an indicator of the LLPT. NMR and dielectric spectroscopy, probing diffusion and rotational dynamics, can provide evidence of a change of behavior on changing  $N$ . (v) By using an inert pressure medium as described above, the pressure of a droplet of fixed  $N$  could be tuned through  $P_c$ . Close to  $T_c$ , monitoring the variations in droplet radius may allow for the direct detection of critical fluctuations.

**Acknowledgments**—We thank the authors of Ref. [18] for providing the data from their simulations shown here in Figs. 1 and 3. We acknowledge useful discussions with P. G. Debenedetti and Barbara Wyslouzil. P. H. P. and I. S.-V. are supported by the Natural Sciences and Engineering Research Council of Canada (NSERC), Grants No. RGPIN-2024-04477 and No. RGPIN-2023-05916, respectively. Computational resources were provided by ACENET (ace-net.ca), a regional partner of the Digital Research Alliance of Canada (alliancecan.ca). F. S. acknowledges support from MIUR-PRIN 2022JWAF7Y, Cineca ISCRA initiative and ICSC-Centro Nazionale di Ricerca in High Performance Computing, Big Data and Quantum Computing, funded by the European Union “NextGenerationEU”.

- [1] P. H. Poole, F. Sciortino, U. Essmann, and H. E. Stanley, Phase behaviour of metastable water, *Nature (London)* **360**, 324 (1992).
- [2] O. Mishima and H. E. Stanley, Decompression-induced melting of ice IV and the liquid–liquid transition in water, *Nature (London)* **392**, 164 (1998).
- [3] K. Winkel, E. Mayer, and T. Loerting, Equilibrated high-density amorphous ice and its first-order transition to the low-density form, *J. Phys. Chem. B* **115**, 14141 (2011).
- [4] P. Gallo, K. Amann-Winkel, C. A. Angell, M. A. Anisimov, F. Caupin, C. Chakravarty, E. Lascaris, T. Loerting, A. Z. Panagiotopoulos, J. Russo, J. A. Sellberg, H. E. Stanley, H. Tanaka, C. Vega, L. Xu, and L. G. M. Pettersson, Water: A tale of two liquids, *Chem. Rev.* **116**, 7463 (2016).
- [5] K. H. Kim, A. Späh, H. Pathak, F. Perakis, D. Mariedahl, K. Amann-Winkel, J. A. Sellberg, J. H. Lee, S. Kim, J. Park, K. H. Nam, T. Katayama, and A. Nilsson, Maxima in the thermodynamic response and correlation functions of deeply supercooled water, *Science* **358**, 1589 (2017).
- [6] K. H. Kim *et al.*, Experimental observation of the liquid–liquid transition in bulk supercooled water under pressure, *Science* **370**, 978 (2020).
- [7] K. Amann-Winkel, K. H. Kim, N. Giovambattista, M. Ladd-Parada, A. Späh, F. Perakis, H. Pathak, C. Yang, T. Eklund, T. J. Lane, S. You, S. Jeong, J. H. Lee, I. Eom, M. Kim, J. Park, S. H. Chun, P. H. Poole, and A. Nilsson, Liquid–liquid phase separation in supercooled water from ultrafast heating of low-density amorphous ice, *Nat. Commun.* **14**, 442 (2023).
- [8] V. Holten and M. A. Anisimov, Entropy-driven liquid–liquid separation in supercooled water, *Sci. Rep.* **2**, 713 (2012), 1207.2101.
- [9] V. Holten, C. E. Bertrand, M. A. Anisimov, and J. V. Sengers, Thermodynamics of supercooled water, *J. Chem. Phys.* **136**, 094507 (2012).
- [10] F. Caupin and M. A. Anisimov, Thermodynamics of supercooled and stretched water: Unifying two-structure description and liquid–vapor spinodal, *J. Chem. Phys.* **151**, 034503 (2019).
- [11] P. G. Debenedetti, F. Sciortino, and G. H. Zerze, Second critical point in two realistic models of water, *Science* **369**, 289 (2020).
- [12] F. Sciortino, Y. Zhai, S. L. Bore, and F. Paesani, Constraints on the location of the liquid–liquid critical point in water, *Nat. Phys.* **21**, 480 (2025).
- [13] R. Weldon and F. Wang, Water potential from adaptive force matching for ice and liquid with revised dispersion predicts supercooled liquid anomalies in good agreement with two independent experimental fits, *J. Phys. Chem. B* **128**, 3398 (2024).
- [14] O. Mishima and T. Sumita, Equation of state of liquid water written by simple experimental polynomials and the liquid–liquid critical point, *J. Phys. Chem. B* **127**, 1414 (2023).
- [15] J. R. Espinosa, J. L. F. Abascal, L. F. Sedano, E. Sanz, and C. Vega, On the possible locus of the liquid–liquid critical point in real water from studies of supercooled water using the TIP4P/Ice model, *J. Chem. Phys.* **158** (2023).
- [16] S. M. A. Malek, P. H. Poole, and I. Saika-Voivod, Thermodynamic and structural anomalies of water nanodroplets, *Nat. Commun.* **9**, 2402 (2018).
- [17] J. L. F. Abascal and C. Vega, A general purpose model for the condensed phases of water: TIP4P/2005, *J. Chem. Phys.* **123**, 234505 (2005).
- [18] J. Weis, F. Sciortino, A. Z. Panagiotopoulos, and P. G. Debenedetti, Liquid–liquid criticality in the wail water model, *J. Chem. Phys.* **157**, 024502 (2022).
- [19] Y. Li, J. Li, and F. Wang, Liquid–liquid transition in supercooled water suggested by microsecond simulations, *Proc. Natl. Acad. Sci. U.S.A.* **110**, 12209 (2013).
- [20] E. R. Pinnick, S. Erramilli, and F. Wang, Predicting the melting temperature of ice–ih with only electronic structure information as input, *J. Chem. Phys.* **137**, 014510 (2012).
- [21] M. J. Abraham, T. Murtola, R. Schulz, S. Páll, J. C. Smith, B. Hess, and E. Lindahl, Gromacs: High performance molecular simulations through multi-level parallelism from laptops to supercomputers, *SoftwareX* **1**, 19 (2015).
- [22] S. Pronk, S. Páll, R. Schulz, P. Larsson, P. Bjelkmar, R. Apostolov, M. R. Shirts, J. C. Smith, P. M. Kasson, D. van der Spoel, B. Hess, and E. Lindahl, GROMACS 4.5: A high-throughput and highly parallel open source molecular simulation toolkit, *Bioinformatics* **29**, 845 (2013).
- [23] B. Hess, C. Kutzner, D. van der Spoel, and E. Lindahl, GROMACS 4: Algorithms for highly efficient, load-balanced, and scalable molecular simulation, *J. Chem. Theory Comput.* **4**, 435 (2008).
- [24] D. van der Spoel, E. Lindahl, B. Hess, G. Groenhof, A. E. Mark, and H. J. C. Berendsen, GROMACS: Fast, flexible, and free, *J. Comput. Chem.* **26**, 1701 (2005).

- [25] E. Lindahl, B. Hess, and D. van der Spoel, GROMACS 3.0: A package for molecular simulation and trajectory analysis, *Mol. Model. Annu.* **7**, 306 (2001).
- [26] H. Berendsen, D. van der Spoel, and R. van Drunen, Gromacs: A message-passing parallel molecular dynamics implementation, *Comput. Phys. Commun.* **91**, 43 (1995).
- [27] S. Nosé, A molecular dynamics method for simulations in the canonical ensemble, *Mol. Phys.* **52**, 255 (1984).
- [28] W. G. Hoover, Canonical dynamics: Equilibrium phase-space distributions, *Phys. Rev. A* **31**, 1695 (1985).
- [29] U. Essmann, L. Perera, M. L. Berkowitz, T. Darden, H. Lee, and L. G. Pedersen, A smooth particle mesh Ewald method, *J. Chem. Phys.* **103**, 8577 (1995).
- [30] See Supplemental Material at <http://link.aps.org/supplemental/10.1103/PhysRevLett.134.138001> for additional simulation details, analysis and results.
- [31] P. H. Poole, S. R. Becker, F. Sciortino, and F. W. Starr, Dynamical behavior near a liquid–liquid phase transition in simulations of supercooled water, *J. Phys. Chem. B* **115**, 14176 (2011).
- [32] S. M. A. Malek, F. Sciortino, P. H. Poole, and I. Saika-Voivod, Evaluating the Laplace pressure of water nanodroplets from simulations, *J. Phys. Condens. Matter* **30**, 144005 (2018).
- [33] R. Weldon and F. Wang, Water potential from adaptive force matching for ice and liquid with revised dispersion predicts supercooled liquid anomalies in good agreement with two independent experimental fits, *J. Phys. Chem. B* **128**, 3398 (2024).
- [34] A. Manka, H. Pathak, S. Tanimura, J. Wölk, R. Strey, and B. E. Wyslouzil, Freezing water in no-man’s land, *Phys. Chem. Chem. Phys.* **14**, 4505 (2012).
- [35] A. J. Amaya, H. Pathak, V. P. Modak, H. Laksmono, N. D. Loh, J. A. Sellberg, R. G. Sierra, T. A. McQueen, M. J. Hayes, G. J. Williams, M. Messerschmidt, S. Boutet, M. J. Bogan, A. Nilsson, C. A. Stan, and B. E. Wyslouzil, How cubic can ice be?, *J. Phys. Chem. Lett.* **8**, 3216 (2017).
- [36] A. J. Amaya and B. E. Wyslouzil, Ice nucleation rates near  $\sim 225$  K, *J. Chem. Phys.* **148**, 084501 (2018).